Computational Materials Science 216 (2023) 111828

Contents lists available at ScienceDirect

Computational Materials Science

journal homepage: www.elsevier.com/locate/commatsci

Full length article

In search of the ground-state crystal structure of Ta_2O_5 from ab initio and Monte Carlo simulations

Andrea Pedrielli [a,b], Nicola M. Pugno [b,c], Maurizio Dapor [a,d], Simone Taioli [a,d,e,*]

[a] European Centre for Theoretical Studies in Nuclear Physics and Related Areas (ECT*), Fondazione Bruno Kessler, Trento, Italy
[b] Laboratory for Bioinspired, Bionic, Nano, Meta Materials and Mechanics, Department of Civil, Environmental and Mechanical Engineering, University of Trento, Trento, Italy
[c] School of Engineering and Materials Science, Queen Mary University of London, London, UK
[d] Trento Institute for Fundamental Physics and Applications (TIFPA-INFN), Trento, Italy
[e] Faculty of Applied Physics and Mathematics, Gdańsk University of Technology, Gdańsk, Poland

ARTICLE INFO

Keywords:
Dielectric properties of Ta_2O_5 polymorphs
Ground state structural model of thermally grown tantalum oxide
Reflection energy loss spectra
Time-dependent density functional theory
Hybrid functionals
Charge Transport Monte Carlo approach

ABSTRACT

Tantalum oxides (Ta_2O_5) are characterized by attractive physical and chemical properties, such as high dielectric constants and anti-reflection behaviour. In principle, their electronic properties can be accurately investigated from first-principles simulations. However, the existence of several stable polymorphs of these oxides represents a major difficulty to calculate and disentangle their respective spectral features. To determine the ground-state structure of the thermally grown oxide, we use linear-response time-dependent density functional theory calculations for investigating the energy loss function in the optical limit of various polymorphs. We show that the experimental energy loss signal, extracted from the reflection energy loss spectra (REELS) recorded on a thermally grown thin film, can be rationalized and interpreted by assuming that the γ-phase of Ta_2O_5 represents the underlying structural model of the oxide. We find that the inclusion of both local field effects and spin–orbit coupling is crucial to compute the energy loss function of these materials. Finally, to further validate the γ-Ta_2O_5 polymorph as a model of the experimental tantalum oxide, we compute the REELS spectra using a Monte Carlo approach, finding an excellent agreement with the as-acquired experimental data.

1. Introduction

Tantalum pentoxide (Ta_2O_5) is a transition-metal oxide with a broad range of attractive characteristics such as high-dielectric and anti-reflection properties as well as wear resistance, thermal and chemical stability. Metal oxide semiconductor (CMOS) technology, optical coatings and photocatalysis are only a few among the many areas of application of these materials. Recently, also the existence of stable Ta_2O_5 nanoparticles has been confirmed; moreover, they have been proposed as possible enhancers of the relative biological effectiveness (RBE) in hadrontherapy for cancer treatment [1].

In all these applications the accurate assessment of the electronic excitation spectra is a key factor, which can be accomplished by using ab initio simulations [2] or experiments [3]. Using the former approach, a key ingredient is the structural atomic arrangement. However, the characterization of the ground-state geometry of bulk Ta_2O_5, which is characterized by a rich crystal polymorphism [4] (meaning that a solid compound can exist and sometimes coexist in more than one atomic arrangement) is a long standing problem in materials science. While crystal polymorphism is common in solids, the number of crystalline and amorphous metastable phases of Ta_2O_5 are relevant, and make the phase diagram entangled and rather complex. It can be found indeed in both amorphous and polycrystalline arrangements, whereby several crystal structures coexist, such as β-Ta_2O_5 [5], β'-Ta_2O_5 [6], β_R-Ta_2O_5 [7], δ-Ta_2O_5 [8] and λ-Ta_2O_5 [9]. Thus, the identification of a structural model of the most stable configuration of Ta_2O_5 to which the relevant electronic and optical properties obtained by experimental measurements are attributed is cumbersome. In particular, it is still debated how to relate the Ta_2O_5 polymorphs to the experimental structural information [10]. Recently, in this respect, a further low-energy structure – the so-called γ-Ta_2O_5 [11,12] – has been proposed. However, the reliability of this structural model to interpret the experimental spectral data is still to be thoroughly investigated.

In order to find the best representative of the ground-state structure of the thermally grown oxide among several Ta_2O_5 stable polymorphs, in this work we aim to show first that a general computational framework can be devised, in which classical transport Monte Carlo (TMC) is coupled with ab initio calculations of the energy loss function (ELF)

---

[*] Corresponding author at: European Centre for Theoretical Studies in Nuclear Physics and Related Areas (ECT*), Fondazione Bruno Kessler, Trento, Italy.
E-mail address: taioli@ectstar.eu (S. Taioli).

https://doi.org/10.1016/j.commatsci.2022.111828
Received 20 March 2022; Received in revised form 23 September 2022; Accepted 26 September 2022

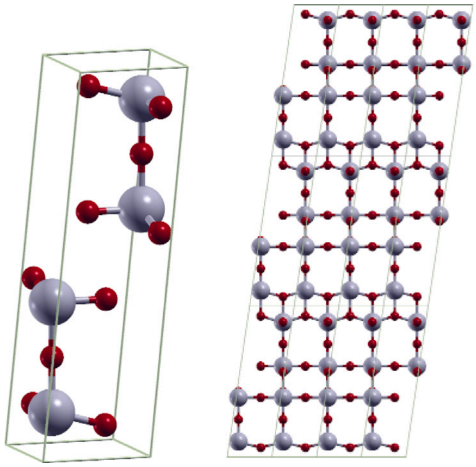

Fig. 1. Unit cell of the γ-Ta_2O_5 polymorph (left) and the corresponding 4 × 3 supercell structure (right). The oxygen atoms are rendered in red, the tantalum atoms in grey.

to determine the ground-state arrangement of materials characterized by a complex phase diagram.

In particular, we study the dielectric properties of the bulk tantalum oxides, which are characterized by complex polymorphism. We reckon the ELFs (that is $\mathrm{Im}(-1/\bar{\epsilon})$, where $\bar{\epsilon}$ is the macroscopic dielectric function defined below), which represent the fingerprint of the material under investigation, of several Ta_2O_5 polymorphs and we compare them with the ELF derived from experimental reflection energy loss spectra (REELS) of the thermally grown oxide via reverse quantitative analysis [3]. Moreover, we apply such a framework to determine the optimal ground-state model of the Ta_2O_5 thermal oxide among the several existing polymorphs. We show by using time-dependent density functional theory (TDDFT) coupled to a TMC scheme that the γ-Ta_2O_5 polymorph is the only atomic arrangement that captures all the features of the as-recorded experimental REEL data, confirming that this crystalline form may represent the most reliable model of tantalum pentoxide grown via thermal oxidation. To compare directly the computed spectrum with the measured energy loss lineshape [3], avoiding background subtraction [13] – a procedure not free from uncertainty – we further check our findings by computing the REEL spectrum using TMC simulations. To carry out these calculations, we need to assess the elastic and inelastic scattering cross sections of the γ-Ta_2O_5 polymorph, which we obtain by using the dielectric [14–16] and Mott [17] theories, respectively. Finally, we demonstrate that the inclusion of both local field effects (LFE), which are crucial in the assessment of the reflectivity and absorbance in materials with strong spatial inhomogeneity, and spin–orbit (SO) coupling is necessary to accurately compute the ELF of these materials.

2. Materials and methods

2.1. Materials structure

The following polymorphs were investigated in this work: β-Ta_2O_5 [5], β'-Ta_2O_5 [6], β_R-Ta_2O_5 [7], δ-Ta_2O_5 [8], λ-Ta_2O_5 [9], and γ-Ta_2O_5 [10] (the atomic coordinates used here are reported in these references). In particular, the unit cell of the γ-Ta_2O_5 polymorph is plotted in Fig. 1. This crystal has a I41/amd symmetry, that is a tetragonal structure, which can be seen more clearly in the 4 × 3 supercell reported in the right panel of Fig. 1. Atomic units are used throughout.

2.2. Dielectric function

The materials microscopic dielectric function can be reckoned by knowing the bare Coulomb potential v_C and the polarization function $\chi(\mathbf{q}, W)$ through [18,19]:

$$\epsilon(\mathbf{q}, W) = 1 - v_C(\mathbf{q})\chi(\mathbf{q}, W). \tag{1}$$

The latter can be in turn obtained by solving the following Dyson-like equation:

$$\chi^{-1}(\mathbf{q}, W) = \chi_0^{-1}(\mathbf{q}, W) - v_C(\mathbf{q}) - f_{xc}(\mathbf{q}, W), \tag{2}$$

where $\chi_0^{-1}(\mathbf{q}, W)$ is the non-interacting (or independent-particle) polarization obtained from the Kohn–Sham wavefunctions and $f_{xc}(\mathbf{q}, W)$ is the energy and momentum dependent TDDFT kernel. In this regard, we have used the adiabatic local density approximation (ALDA) kernel, which is related to the LDA exchange–correlation functional $v_{xc}[\rho]$ by:

$$f_{xc}(\mathbf{r}, t) = \left\{ \frac{d}{d\rho} v_{xc}[\rho] \right\}_{\rho=\rho(\mathbf{r},t)}, \tag{3}$$

where ρ is the DFT ground-state density.

For periodic crystals one can exploit the translational symmetry, which allows one to write conveniently the microscopic dielectric function in the reciprocal space as a matrix, i.e. $\epsilon_{\mathbf{G},\mathbf{G}'}(\mathbf{q}, W) = \epsilon(\mathbf{q}+\mathbf{G}, \mathbf{q}+\mathbf{G}', W)$, where $\mathbf{G}$ and $\mathbf{G}'$ are reciprocal lattice vectors, and $\mathbf{q}$ is the transferred momentum vector in the first Brillouin zone.

The measured macroscopic dielectric function $\bar{\epsilon}(\mathbf{q}, W)$ and the computed microscopic function $\epsilon_{\mathbf{G},\mathbf{G}'}(\mathbf{q}, W)$ are related by the following expression [20]:

$$\bar{\epsilon}(\mathbf{q}, W) = \left[\epsilon^{-1}_{\mathbf{G}=0,\mathbf{G}'=0}(\mathbf{q}, W)\right]^{-1}. \tag{4}$$

LFE were included here by inverting the full dielectric matrix and then taking the head element of the inverse matrix.

2.3. Energy loss function

To describe the propagation of charged particles through matter using the dielectric formalism [15], one relies on the ELF of the material, which is related to the macroscopic dielectric function as follows:

$$\mathrm{ELF} = \mathrm{Im}\left[\frac{-1}{\bar{\epsilon}(\mathbf{q}, W)}\right]. \tag{5}$$

Here, we carry out the ab initio calculation of the ELF in the optical limit ($\mathbf{q} \to 0$), and we compare it with the available experimental optical data. The dielectric response function in the optical limit has been obtained using the linear response TDDFT implementation of the ELK code suite [21] on top of the DFT ground state. ELK uses an all-electron Full-Potential Linearized Augmented-Plane-Wave (FP-LAPW) approach, which avoids any approximation related to the use of the pseudopotential describing the ion-electron interaction.

The calculations were carried out in spin-polarized mode so as to include SO coupling. The local spin density approximation (LSDA) exchange–correlation functional [22] has been used for the ground-state calculations alongside the ALDA approximation for the time-dependent exchange–correlation kernel.

A 4 × 4 × 2 k-point grid for γ-Ta_2O_5 and β-Ta_2O_5 and a 4 × 2 × 2 k-point grid for the other polymorphs have been used. A number of empty bands equal to 60 for each atom have been employed to obtain converged results up to 80 eV. The ELF spectra were finally averaged over the three components of the polarization vector of the external electromagnetic field.

2.4. Extension of the energy loss function

To run our TMC scheme for modelling the energy loss spectra of tantalum pentoxides, we need first to determine the inelastic and elastic scattering cross sections. The former can be obtained by knowing the dependence of the ELF over the entire spectrum of excitation energies W and momentum transfers $\mathbf{q}$ [2,23–26]. Ab initio calculations of the ELF on a large energy range are prohibitive owing to the high computational cost of including many electronic transitions to the excited states. Thus, while first-principles can be used for computing the ELF below 100 eV, its extension along the excitation energy axis has been performed by using the experimental NIST X-ray atomic data up to 30 keV [27]. The ab initio and experimental ELFs in the optical limit were matched smoothly and were fitted by Drude–Lorentz functions coupled with a momentum dependent broadening γ_i, which takes into account the momentum dispersion of the electronic excitation. To include inner-shell electronic excitations in the computation of the ELF we add Drude–Lorentz functions multiplied by a switching function F, in order to reproduce the sharp edges of core excitations:

$$\mathrm{Im}\left[\frac{-1}{\bar{\epsilon}(\mathbf{q}=0,W)}\right] = \\ = \sum_i \frac{A_i \gamma_i W}{(W_i^2 - W^2)^2 + (\gamma_i W)^2} \cdot F(W,B_i), \tag{6}$$

where:

$$F(W,B_i) = \begin{cases} 1 \text{ for outer electrons} \\ \frac{1}{1+e^{-(W-B_i)}} \text{ for core electrons.} \end{cases} \tag{7}$$

In Eqs. (6)–(7) A_i, W_i, and γ_i, B_i are fitting parameters, which physically represent the intensity, energy position, and width of the transitions. Finally, the momentum dispersion is introduced by [16]:

$$W_i(q) = \sqrt{W_i{}^2 + (12/5) \cdot \mathrm{E_f} \cdot q^2/2 + q^4/4} \\ \gamma_i(q) = \sqrt{\gamma_i{}^2 + q^2/2 + q^4/4}, \tag{8}$$

where E_f is the Fermi energy. The parameters $B_i(q)$ have the same dispersion of $W_i(q)$ for consistency.

2.5. Monte Carlo simulations of electron transport

With the ELF extension in place, TMC inputs, such as the inelastic scattering cross section, can be obtained. In the TMC method, electrons are considered as point particles following classical trajectories that are induced by elastic and inelastic interactions. The elastic and inelastic scattering processes are dealt with quantum mechanics. The occurrence probabilities of elastic and inelastic interactions at a certain kinetic energy T can be calculated, respectively, by $p_{\mathrm{el}}(T) = \Lambda_{\mathrm{el}}(T)/\Lambda_{\mathrm{tot}}(T)$ and $p_{\mathrm{inel}}(T) = \Lambda_{\mathrm{inel}}(T)/\Lambda_{\mathrm{tot}}(T)$, where $\Lambda_{\mathrm{tot}}(T) = \Lambda_{\mathrm{inel}}(T) + \Lambda_{\mathrm{el}}(T)$ and $\Lambda_{\mathrm{el/inel}} = \lambda^{-1}_{\mathrm{el/inel}}(T)$ is the inverse mean free path for the elastic or inelastic scattering [28–31]. The TMC method proceeds by selecting a particular interaction event by comparing a random number uniformly distributed in the range $[0,1]$ with the relevant probability.

In particular, the energy loss W suffered by electrons with kinetic energy T upon inelastic scattering events can be reckoned by equating the inelastic scattering cumulative probability distribution to a uniformly-distributed random number in the range $[0,1]$, as follows:

$$P_{\mathrm{inel}}(T,W) = \frac{1}{\Lambda_{\mathrm{inel}}(T)} \int_0^W \frac{d\Lambda_{\mathrm{inel}}(T,W')}{dW'} dW'. \tag{9}$$

Other than the energy loss, the angular deviation due to inelastic scattering events is evaluated according to the classical binary collision theory [28–31]. In Eq. (9) the integrand is the differential inverse inelastic mean free path (DIIMFP):

$$\frac{d\Lambda_{\mathrm{inel}}(T,W)}{dW} = \frac{1}{\pi T} \int_{q_-}^{q_+} \frac{1}{q} \mathrm{Im}\left[\frac{-1}{\bar{\epsilon}(\mathbf{q},W)}\right] dq, \tag{10}$$

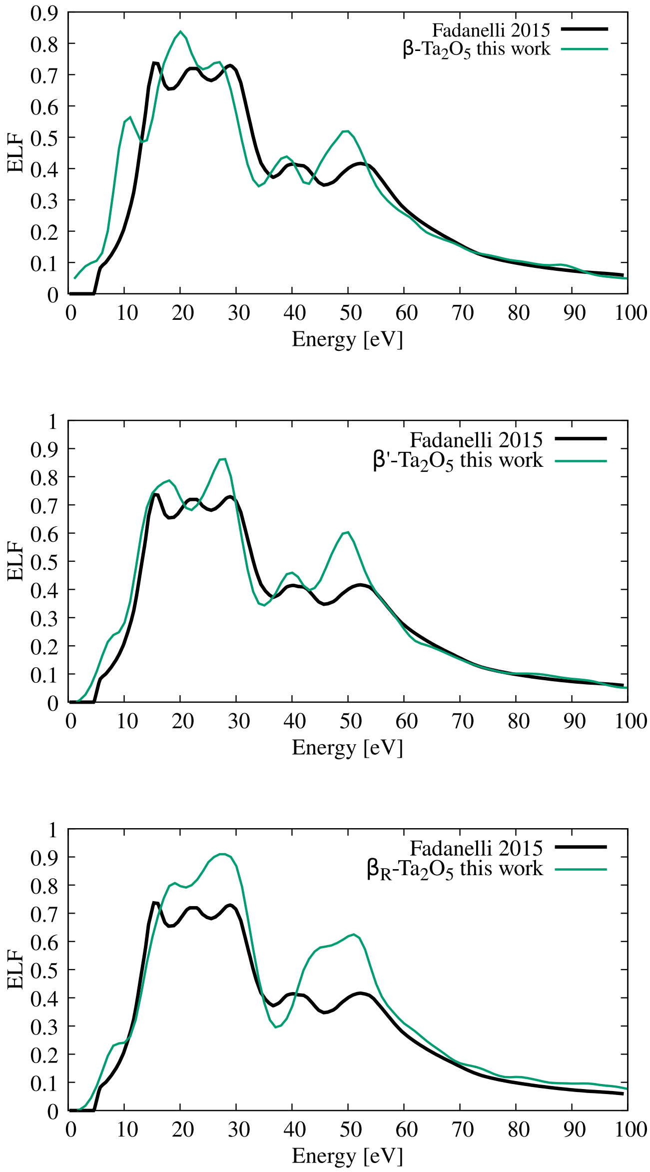

Fig. 2. ELF of β-Ta$_2$O$_5$, β'-Ta$_2$O$_5$, β_{R}-Ta$_2$O$_5$ polymorphs in comparison with experimental data from Ref. [3]. The local spin density approximation (LSDA) to the exchange–correlation functional has been used to include SO coupling alongside the ALDA approximation to the time-dependent exchange–correlation kernel.

where the integration limits, $q_\pm = \sqrt{2T} \pm \sqrt{2(T-W)}$, result from momentum conservation during the interaction process.

From the DIIMFP the inelastic mean free path (IMFP) can be derived. The latter is defined as the inverse of the inelastic scattering cross section:

$$\Lambda_{\mathrm{inel}}(T) = \int_{W_{\mathrm{min}}}^{W_{\mathrm{max}}} \frac{d\Lambda_{\mathrm{inel}}(T,W)}{dW} dW, \tag{11}$$

where the integration limit W_{min} is set to E_{gap} for semiconductors and insulating materials, while W_{max} represents the minimum between T and $(T + W_{\mathrm{min}})/2$. We note that surface plasmon excitations are not taken into account.

The second key quantity to run TMC simulations in solids is the elastic scattering cumulative probability. In this respect, the angular deviation of the electron trajectories following an elastic collision in terms of the scattering angle θ is

$$P_{\mathrm{el}}(T,\theta) = \frac{2\pi}{\Lambda_{\mathrm{el}}(T)} \int_0^\theta \frac{d\Lambda_{\mathrm{el}}(T,\theta')}{d\Omega} \sin\theta' d\theta'. \tag{12}$$

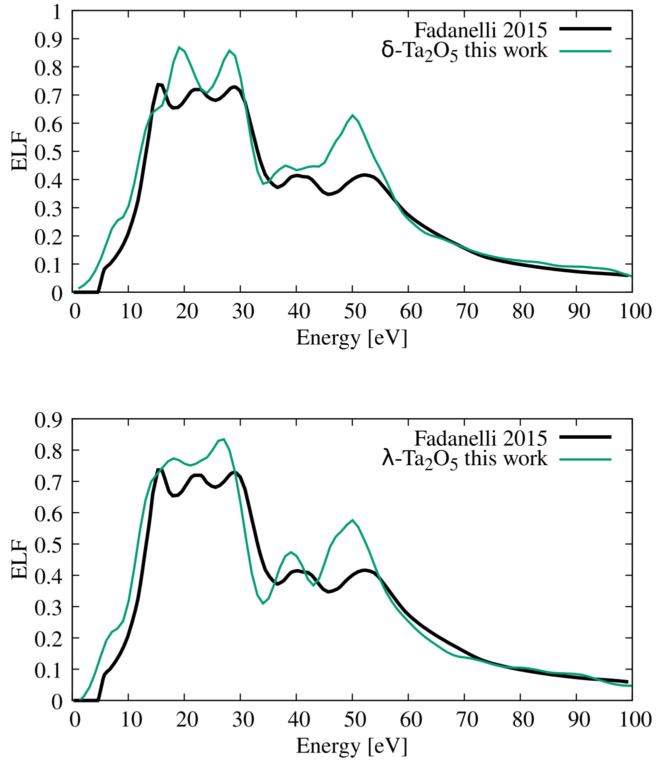

Fig. 3. ELF of δ-Ta_2O_5 and λ-Ta_2O_5 polymorphs in comparison with experimental data from Ref. [3]. The local spin density approximation (LSDA) to the exchange–correlation functional has been used to include SO coupling alongside the ALDA approximation to the time-dependent exchange–correlation kernel.

θ can be evaluated by equating this cumulative probability to a uniformly distributed random number generated in the range $[0, 1]$. Electrons do not suffer energy loss during an elastic collision.

The elastic scattering is accounted for by means of the Mott theory [17]. This approach provides the differential elastic scattering cross-section (DESCS) for an electron impinging on a central potential and subsequently scattered by an angle θ as follows [28–31]:

$$\frac{d\Lambda_{\mathrm{el}}(T,\theta)}{d\Omega} = \mathcal{N}\sum_{m,n} e^{(i\mathbf{q}\cdot\mathbf{r}_{mn})}\left[f_m(\theta)f_n^*(\theta) + g_m(\theta)g_n^*(\theta)\right], \tag{13}$$

where $\mathbf{r}_{mn} = \mathbf{r}_m - \mathbf{r}_n$, and $\mathbf{r}_m$ $(\mathbf{r}_n)$ identifies the position of the m^{th} (n^{th}) atom in the periodic unit cell, $\mathcal{N}$ is the target atomic number density, $f_{m(n)}(\theta)$ and $g_{m(n)}(\theta)$ are the direct and spin–flip scattering amplitudes of the m^{th}–atom (and of the neighbouring n^{th}–atom), respectively, which can be obtained by solving the Dirac equation in a central atomic field. Eq. (13) generalizes the Mott theory for the scattering from atomic targets by taking into account the presence of bonded interactions among neighbours in the periodic unit cell. Indeed, by allowing interference between the direct and spin–flip scattering amplitudes condensed phase effects can be included in the assessment of the elastic scattering cross section.

Finally, by integrating over the solid angle one obtains the total elastic scattering cross section:

$$\Lambda_{\mathrm{el}}(T) = \int_{\Omega}\frac{d\Lambda_{\mathrm{el}}(T,\theta)}{d\Omega}d\Omega. \tag{14}$$

The calculation of the DESCS has been performed using the ELSEPA code [32] with a $2 \times 2 \times 1$ supercell to account for crystalline effects over the elastic scattering cross section.

The TMC calculations have been performed using the in-house SEED code [28–31]. The electron trajectories ensemble is set to reach statistical significance and a low-noise-to-signal ratio of the simulated data ($\approx 10^9$ trajectories). The full width at half maximum (FWHM) of the elastic peak has been set to 0.8 eV in order to match the experimental linewidth.

3. Results and discussion

3.1. Energy loss function from ab initio calculations

As many different structural models were reported for Ta_2O_5, we investigate here the ELF of the most relevant geometries. This quantity is indeed a relevant marker that can be compared with available experimental data for the identification of the thermally-grown oxide ground-state atomic structure.

We report in Figs. 2 and 3 the comparison of our calculated ELFs of several polymorphs with those that have been obtained from the REEL raw experimental data recorded on a Ta_2O_5 sample by reverse quantitative analyses of the electron energy loss spectra using the QUEELS code [3]. We notice that the sample under investigation [3] is a 50 nm thick layer of Ta_2O_5 that was grown on a Ta substrate by thermal oxidation at 600 °C upon oxygen irradiation. The ELF of the γ-Ta_2O_5 phase is reported in Fig. 4, where a rigid blueshift of 1.5 eV (see further below for a discussion of such rigid shift) has been applied to our calculated data to align them with the results refined using the QUEELS software package from the experimental REELS. This shift can be rationalized so as to correct the well-known underestimation of the band gap, which impacts the ELF calculations via Eq. (11), using the LDA (2.98 eV in this work) and PBE functionals (2.26 eV [11]) with respect to higher accuracy approaches, such as the HSE06 (3.75 eV) and PBE0 (4.51 eV) hybrid functionals [11]. From absorbance measurements, values ranging from 4.2 to 4.4 eV for amorphous films and 3.9 to 4.5 eV for crystalline films were obtained [33].

We note that hybrid functionals to model the electron–electron interaction may generally lead to a better agreement of the computed band gaps with the experimental data. However, we point out that in the case of the γ-Ta_2O_5 polymorph, the discrepancy between computed and experimental band gap is actually significant or, at least, not negligible also when using hybrid functionals. Indeed HSE06 [34] delivers a band gap of 3.75 eV (to be compared with an average experimental gap of $\simeq$4.2 eV for crystalline films of Ta_2O_5), while PBE0 [35] delivers a different value of the band gap (4.5 eV), so their results are inconsistent with each other.

A possibility arises to use the family of HSE screening exchange functionals, which improve computational efficiency by using a screened Coulomb potential, by modifying the exchange portion of the energy. HSE functionals are implemented in the pseudopotential, plane wave Quantum Espresso suite [36]. An almost perfect agreement (4.1 eV) of the γ-Ta_2O_5 band gap with the experimental data ($\simeq$4.2 eV) was achieved using the HSE functional by tuning both the mixing parameter, determining the exchange portion of the HF exchange energy ($a = 0.5$), and an adjustable parameter ($\omega = 0.2$), controlling the short-rangeness of the interaction [34]. We are reminded that the exchange–correlation potential referred to as HSE06 is characterized by $a = 0.25$.

Nevertheless, to achieve convergence of the electronic ground state, we experienced an increase by two orders of magnitude in the computational time. In particular, the converged band structure calculation of the γ-phase polymorph with standard PBE exchange–correlation potential takes only CPU minutes on 256 state-of-the-art processors, while using HSE takes a few CPU hours on the same number and type of processors. Thus, the use of such hybrid functionals to screen the ELF for different phases of materials characterized by a large number of polytypes is severely limited by the computational cost. Furthermore, we could not reproduce the band gap of the γ-Ta_2O_5 phase using different values of the $\omega = 0.2$ and $a = 0.5$ parameters, which may represent also a limit to the predictability of first-principles simulations unless an a priori determination of the weight of each individual component of the exchange–correlation functional (instead of fitting some generic experimental data) can be achieved. However, the application of a rigid shift to the ELF, supported on the basis of the calculations performed by using the HSE exchange–correlation interaction which delivers a correct band gap, leads to the accurate interpretation of the EELS experimental measurements.

We also point out that a main goal of our analysis is to determine the ground-state structure of the thermal oxide among the Ta_2O_5 polymorphs by using their dielectric properties as a guiding light, most notably the energy loss spectra. The input values by which we feed our charge TMC simulations, such as the inelastic scattering cross section, are crucially affected by the spectral behaviour of the ELF lineshape, which is well described within LSDA+ALDA in comparison to the experimental data, rather than by the size of such shift (of course, to some extent). Indeed, other critical points to determine the ELF with high accuracy are the inclusion of LFE and SO coupling.

Finally, while hybrid functionals deliver band gaps closer to the experiments, the electronic structure calculations would still be carried out on the γ-phase unit cell. The latter, while capturing most of the features of the experimental oxide, is of course a simplified model of the actual polycrystalline oxides used in the experimental measurements, which cannot be accounted for within a first-principles framework, owing to the computational cost scaling at least cubically with the system size. Thus, in the following analysis the screening of different crystal structures in order to find the most suitable ground-state geometry to describe the experimental oxide is carried out within the LSDA+ALDA scheme, which is a computationally effective and solidly justified approximation.

We notice that in the top panel of Fig. 2 the spectral lineshape derived from experiments presents five well resolved peaks. In particular, the first three peaks in the range 15–35 eV are characterized by a comparable intensity, while those at high energy (> 35 eV) have lower intensity. These characteristics are also reproduced in our calculations (see green lines in Figs. 2 and 3). However, the spectral lineshape of these polymorphs cannot be considered in good agreement with the reference ELF (black line in Figs. 2 and 3). In fact, in the range 15–35 eV none of these structural arrangements deliver the three peaks with similar intensity in the experiments. Furthermore, only β-Ta_2O_5, β'-Ta_2O_5, λ-Ta_2O_5 polymorphs are characterized by two well resolved peaks at higher energy, which are at variance merged in one broad peak for the β_R-Ta_2O_5 phase, while the first of them is almost suppressed in the δ-Ta_2O_5 form.

At odds with these findings, a remarkable agreement with the reference experimental data [3] can be obtained by considering the γ-Ta_2O_5 phase, as shown in Fig. 4. In particular, the three peaks of similar intensity in the range 15–35 eV are recovered, and the two peaks beyond 35 eV are less bright than for the other cases, in better agreement with the ELF experimental data. Moreover, the shoulder at 10 eV, while not so pronounced in the spectra from Ref. [3], is clearly reproduced in our simulations as found in Ref. [37]. We stress that the ELF reported in Ref. [3], which is derived from the REELS experiments by using the QUEELS code, has been corrected at energy larger than 60 eV to fulfil the sum rules, while our ab initio calculations do not need any correction.

We point out that our analysis to determine the most suitable structure to model the experimental spectral features is based not only on the relative distance between the brightest peaks, but also on their relative and absolute intensity in comparison to experimental data. For example, the ELF of the β-Ta_2O_5 polymorph (see Fig. 2) does not reproduce such features well, as it lacks the similar intensity of the main three peaks (15 to 35 eV), being the first one lower and the second higher not to a marginal extent with respect to experimental measurements. Furthermore, the middle peak is far too bright with respect to experiments, while the proposed γ-Ta_2O_5 signals have similar intensities for the three well-resolved peaks.

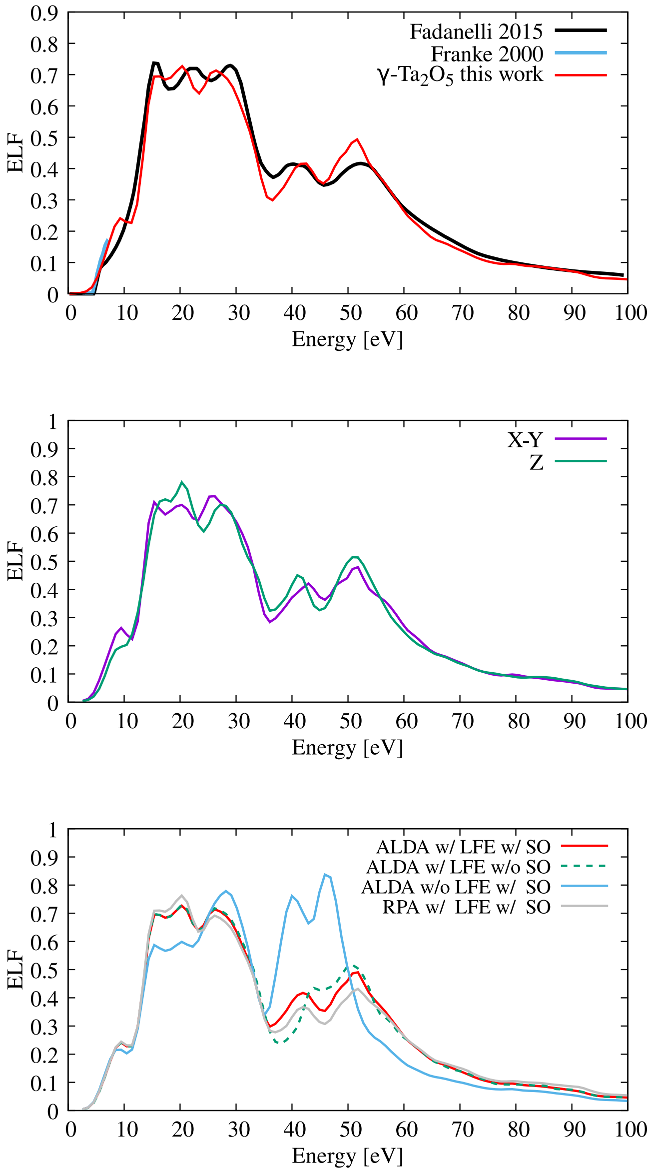

Fig. 4. Top panel: ELF of γ-Ta_2O_5 in comparison with experimental data from Refs. [3,37]. Central panel: Decomposition of the ELF along the polarization directions ($X-Y, Z$). Bottom panel: ELF at different levels of theory. Calculated ELF are blueshifted by 1.5 eV (see the discussion in the main text on such shift).

This overestimation of the ELF of the β-Ta_2O_5 polymorph results also in a discrepancy in the f-sum rule, which typically serves as a check of the accuracy of the optical ELF. The f-sum rule basically integrates with suitable weight the optical ELF giving the effective number of electrons per unit cell participating in the electronic excitations and, thus, should converge to the atomic number. This discrepancy does not occur using our optical ELF of the γ-Ta_2O_5 polymorph, where both the intensity and shape are in good agreement with the experiments. Thus, we conclude that the β-Ta_2O_5 structure, although shifted to match the first peak, seems unsuitable to describe the experimental ELF.

The contribution to the ELF coming from different polarization directions, is reported in Fig. 4 (middle panel). We note that the main features of the ELF are essentially independent on the polarization direction aside from the shoulder at 10 eV and the central peak among the triplets in the range 15–35 eV.

To show the significant impact that the inclusion of both the LFE and the SO coupling has on the calculated lineshape, in the bottom

Table 1
Parameters A_i, W_i, γ_i, and B_i of the Drude–Lorentz fit of the optical ELF.

A_i (eV^2)	W_i (eV)	γ_i (eV)	B_i (eV)
3.2	10.3	2.4	
31.2	16.9	4.3	
76.8	21.7	7.5	
108.8	28.5	8.4	
50.8	32.9	6.2	
47.1	43.0	5.8	
238.7	53.4	13.1	
242.4	64.8	41.4	
1094.2	176.3	391.5	
1545.3	127.6	123.8	544.6
11509.9	306.9	104.4	1783.4
3000.5	482.8	101.8	2274.0

panel of Fig. 4 we report the ELF of the γ-Ta$_2$O$_5$ phase with/without the LFE and the SO coupling, respectively, as well as in the random phase approximation (RPA). We stress that the role of LFE is relevant: they affect all the features of the ELF demonstrating the presence of strong spatial inhomogeneity.

In particular, the LFEs mainly decrease the intensity of the peaks in the range 35–60 eV, showing their fundamental role in reproducing the experimental intensity of the three peaks, while they have a smaller effect on the low energy part of the spectrum. The SO coupling has a less relevant impact on the ELF with respect to the LFE, but it reveals crucial in order to recover the peaks at 35–45 eV. We also notice that the difference in using the ALDA kernel or RPA is essentially negligible both with and without introducing the LFEs.

3.2. *Energy extension and momentum dispersion of the ELF*

To run TMC simulations one needs to determine the dependence of the ELF on the entire spectrum of excitation energies and its dispersion with respect to momentum transfer (the so-called Bethe surface). To achieve this goal we used the Drude–Lorentz model with a momentum dependent broadening discussed in Eqs. (6)–(8). In the top panel Fig. 5 we report the $\log - \log$ plot of the optical ELF and of the fitting Drude functions. The fit parameters A_i, W_i, γ_i, and B_i are reported in Table 1.

A 3D plot of the momentum dispersion of the ELF related to the outer shell excitations is reported in the bottom panel of Fig. 5. While we chose a specific analytical momentum dependence of the ELF (see Eq. (8)), we can consider our findings robust with respect to different dispersion models [23,26], also in view of the relatively high kinetic energy of the impinging electron beam (5 keV). This can be seen for example by computing the IMFP of bulk Ta$_2$O$_5$ (see Eq. (11)), which we report in the top panel of Fig. 6 alongside the data derived from the experiments [3]. We note that the calculated IMFP is in excellent agreement with the experimentally derived one [3] at all energies, although the dispersion relations used are different.

3.3. *Monte Carlo simulations of REEL spectra*

To compare directly the theoretical spectrum with the experimental energy loss lineshape of Ta$_2$O$_5$ [3], rather than with the ELF, which is derived from the former via a subtraction procedure [13], we eventually used TMC simulations. Indeed, to further validate the γ-Ta$_2$O$_5$ form as a good structural model for thermal tantalum oxide we decided to follow the inverse route and compute the REEL spectrum starting form our ab initio ELF to be compared with the experimental measurements, in this way effectively avoiding any subtraction.

In the lower panel of Fig. 6 we report the computed REEL spectrum of bulk γ-Ta$_2$O$_5$ (solid green line) in comparison to the as-measured experimental data [3] (black line), finding an excellent agreement. We indeed reproduce all the main features of the experimental spectrum. The spectra were normalized with respect to the highest energy loss peak.

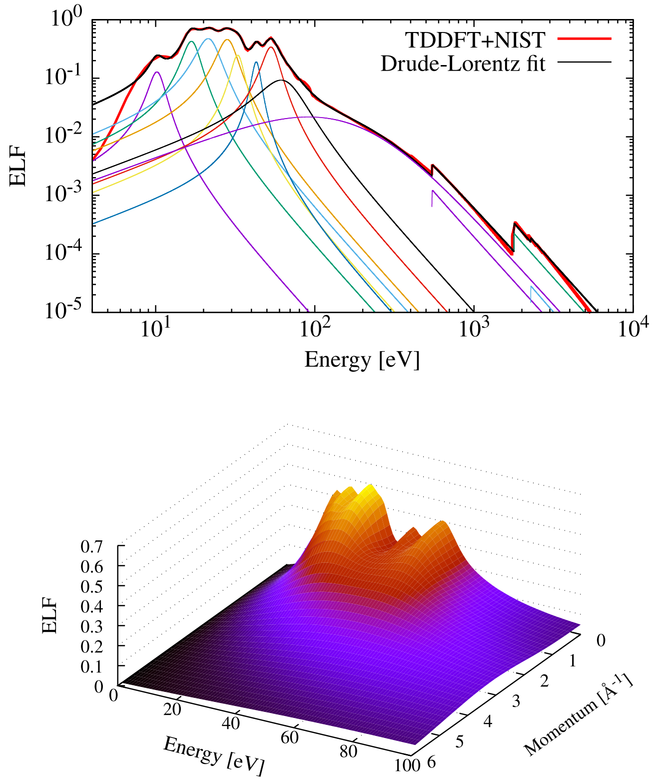

Fig. 5. Top: ELF of the γ-Ta$_2$O$_5$ form in the optical limit and the relevant fitting functions. Bottom: Bethe surface of γ-Ta$_2$O$_5$ as a function of transferred momentum and excitation energy by extending to finite momentum the optical ELF via a momentum dependent Drude–Lorentz model.

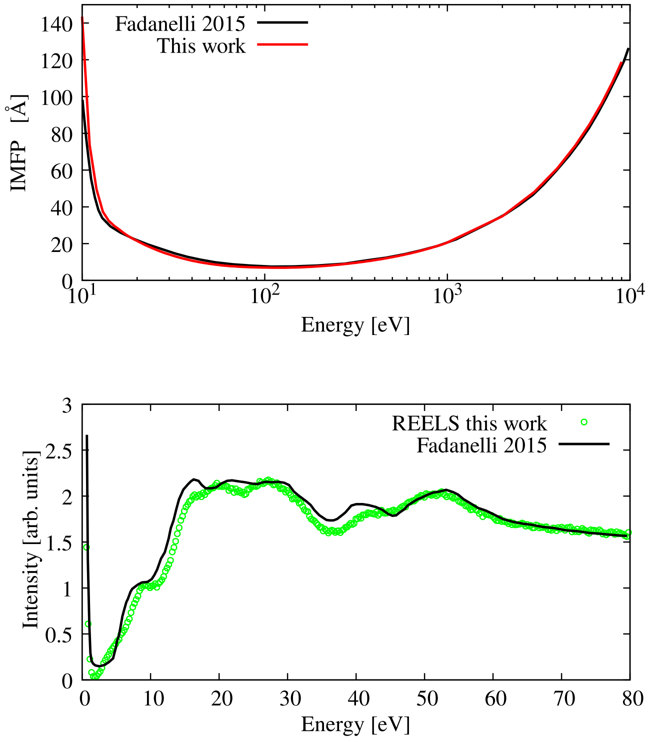

Fig. 6. Top panel: Comparison of our calculation of the IMFP with data from Ref. [3]. Bottom panel: Comparison of our Monte Carlo calculation of the REEL spectrum with experimental data from Ref. [3].

We stress that the very good agreement of our results with experimental REELS on the one hand validates our methodological approach, on the other hand confirms that the γ-Ta_2O_5 polymorph is the most suitable model of tantalum oxide grown by thermal oxidation.

4. Conclusions

In summary, we computed the optical ELF of several polymorphs of Ta_2O_5 using a high-accuracy first-principles linear response TDDFT approach. We showed that the recently proposed γ-Ta_2O_5 polymorph is the most reliable structure in reproducing the ELF experimental lineshape.

Furthermore, we have demonstrated that the inclusion of LFE and SO coupling is fundamental for the description of the electronic structure of these material phases. In order to test our calculations directly against the experimental measurements, thus avoiding any subtraction, we used our ab initio optical ELF and the Drude–Lorentz approach for including the finite transfer momentum dispersion, necessary to calculate the inelastic scattering cross section. We performed TMC simulations of the REEL spectrum of the γ-Ta_2O_5 polymorph finding an excellent agreement with the experimental data. These results represent a striking confirmation that the γ-Ta_2O_5 polymorph is the most suitable model to describe the ground-state structure of tantalum oxide grown by thermal oxidation.

Our findings can be useful to a further investigation of the dielectric properties of tantalum oxides, paving the way towards the application of these materials e.g. as radioenhancers in hadrontherapy for cancer cure.

CRediT authorship contribution statement

Andrea Pedrielli: Conceptualization, Methodology, Investigation, Software, Writing – original draft, Reviewing and editing. **Nicola M. Pugno:** Supervision, Reviewing and editing, Funding acquisition. **Maurizio Dapor:** Supervision, Conceptualization, Methodology, Investigation, Project administration. **Simone Taioli:** Supervision, Conceptualization, Methodology, Writing – original draft, Validation, Reviewing and editing, Project administration, Funding acquisition.

Declaration of competing interest

The authors declare the following financial interests/personal relationships which may be considered as potential competing interests: Simone Taioli reports financial support was provided by Trento and Rovereto Bank Foundation.

Data availability

Data will be made available on request.

Acknowledgements

A. P. acknowledges Fondazione Caritro, Italy and DICAM (University of Trento), Italy for the financial support under the CARITRO project “*High-Z ceramic oxide nanosystems for mediated proton cancer therapy*”.

References

[1] S. McKinnon, S. Guatelli, S. Incerti, V. Ivanchenko, K. Konstantinov, S. Corde, M. Lerch, M. Tehei, A. Rosenfeld, Local dose enhancement of proton therapy by ceramic oxide nanoparticles investigated with Geant4 simulations, Phys. Med. 32 (12) (2016) 1584–1593.

[2] A. Pedrielli, P. de Vera, P.E. Trevisanutto, N.M. Pugno, R. Garcia-Molina, I. Abril, S. Taioli, M. Dapor, Electronic excitation spectra of cerium oxides: from ab initio dielectric response functions to Monte Carlo electron transport simulations, Phys. Chem. Chem. Phys. (2021).

[3] R.C. Fadanelli, M. Behar, L.C.C.M. Nagamine, M. Vos, N.R. Arista, C.D. Nascimento, R. Garcia-Molina, I. Abril, Energy loss function of solids assessed by ion beam energy-loss measurements: Practical application to Ta_2O_5, J. Phys. Chem. C 119 (35) (2015) 20561–20570.

[4] C. Askeljung, B.-O. Marinder, M. Sundberg, Effect of heat treatment on the structure of L-Ta_2O_5: a study by XRPD and HRTEM methods, J. Solid State Chem. (ISSN: 0022-4596) 176 (1) (2003) 250–258.

[5] G.S. Oehrlein, F.M. d’Heurle, A. Reisman, Some properties of crystallized tantalum pentoxide thin films on silicon, J. Appl. Phys. 55 (10) (1984) 3715–3725.

[6] R. Hollerweger, D. Holec, J. Paulitsch, M. Bartosik, R. Daniel, R. Rachbauer, P. Polcik, J. Keckes, C. Krywka, H. Euchner, P. Mayrhofer, Complementary ab initio and X-ray nanodiffraction studies of Ta_2O_5, Acta Mater. (ISSN: 1359-6454) 83 (2015) 276–284.

[7] R. Ramprasad, First principles study of oxygen vacancy defects in tantalum pentoxide, J. Appl. Phys. 94 (9) (2003) 5609–5612.

[8] M. Hiratani, S. Kimura, T. Hamada, S. Iijima, N. Nakanishi, Hexagonal polymorph of tantalum–pentoxide with enhanced dielectric constant, Appl. Phys. Lett. 81 (13) (2002) 2433–2435.

[9] S.-H. Lee, J. Kim, S.-J. Kim, S. Kim, G.-S. Park, Hidden structural order in orthorhombic Ta_2O_5, Phys. Rev. Lett. 110 (23) (2013).

[10] J. Lee, W. Lu, E. Kioupakis, Electronic properties of tantalum pentoxide polymorphs from first-principles calculations, Appl. Phys. Lett. 105 (20) (2014) 202108.

[11] Y. Yang, Y. Kawazoe, Prediction of new ground-state crystal structure of Ta_2O_5, Phys. Rev. Mater. 2 (2018) 034602.

[12] J.-H. Yuan, K.-H. Xue, Q. Chen, L.R.C. Fonseca, X.-S. Miao, Ab initio simulation of Ta_2O_5: A high symmetry ground state phase with application to interface calculation, Ann. Phys. 531 (8) (2019) 1800524.

[13] S. Tougaard, F. Yubero, QUEELS software package for calculation of surface effects in electron spectra, Surf. Interface Anal. 36 (8) (2004) 824–827.

[14] R.H. Ritchie, Plasma losses by fast electrons in thin films, Phys. Rev. 106 (1991) 874–881.

[15] R.H. Ritchie, Interaction of charged particles with a degenerate Fermi-Dirac electron gas, Phys. Rev. 114 (1959) 644–654.

[16] R.H. Ritchie, A. Howie, Electron excitation and the optical potential in electron microscopy, Phil. Mag. 36 (2) (1977) 463–481.

[17] N.F. Mott, The scattering of fast electrons by atomic nuclei, Proc. R. Soc. Lond. Ser. A 124 (1929) 425–442.

[18] G. Onida, L. Reining, A. Rubio, Electronic excitations: density-functional versus many-body Green’s-function approaches, Rev. Modern Phys. 74 (2002) 601–659.

[19] H.-C. Weissker, J. Serrano, S. Huotari, E. Luppi, M. Cazzaniga, F. Bruneval, F. Sottile, G. Monaco, V. Olevano, L. Reining, Dynamic structure factor and dielectric function of silicon for finite momentum transfer: Inelastic X-ray scattering experiments and ab initio calculations, Phys. Rev. B 81 (2010) 085104.

[20] N. Wiser, Dielectric constant with local field effects included, Phys. Rev. 129 (1963) 62–69.

[21] ELK website URL http://elk.sourceforge.net/.

[22] J.P. Perdew, Y. Wang, Accurate and simple analytic representation of the electron-gas correlation energy, Phys. Rev. B 45 (23) (1992) 13244–13249.

[23] M. Azzolini, T. Morresi, G. Garberoglio, L. Calliari, N.M. Pugno, S. Taioli, M. Dapor, Monte Carlo simulations of measured electron energy-loss spectra of diamond and graphite: role of dielectric-response models, Carbon 118 (2017) 299.

[24] M. Azzolini, T. Morresi, K. Abrams, R. Masters, N. Stehling, C. Rodenburg, N.M. Pugno, S. Taioli, M. Dapor, Anisotropic approach for simulating electron transport in layered materials: computational and experimental study of highly oriented pyrolitic graphite, J. Phys. Chem. C 122 (18) (2018) 10159–10166.

[25] S. Taioli, P.E. Trevisanutto, P. de Vera, S. Simonucci, I. Abril, R. Garcia-Molina, M. Dapor, Relative role of physical mechanisms on complex biodamage induced by carbon irradiation, J. Phys. Chem. Lett. 12 (1) (2020) 487–493.

[26] M. Azzolini, O.Y. Ridzel, P.S. Kaplya, V. Afanas’ev, N.M. Pugno, S. Taioli, M. Dapor, A comparison between Monte Carlo method and the numerical solution of the ambartsumian-chandrasekhar equations to unravel the dielectric response of metals, Comput. Mater. Sci. 173 (2020) 109420.

[27] S. Seltzer, X-ray form factor, attenuation and scattering tables, NIST standard reference database 66, 1995.

[28] S. Taioli, S. Simonucci, M. Dapor, SURPRISES: when ab initio meets statistics in extended systems, Comput. Sci. Discov. 2 (1) (2009) 015002.

[29] S. Taioli, S. Simonucci, L. Calliari, M. Filippi, M. Dapor, Mixed ab initio quantum mechanical and Monte Carlo calculations of secondary emission from SiO_2 nanoclusters, Phys. Rev. B 79 (8) (2009) 085432.

[30] S. Taioli, S. Simonucci, L. Calliari, M. Dapor, Electron spectroscopies and inelastic processes in nanoclusters and solids: Theory and experiment, Phys. Rep. 493 (5) (2010) 237–319.

[31] M. Dapor, Transport of Energetic Electrons in Solids. Computer Simulation with Applications to Materials Analysis and Characterization, 3rd Ed., Springer Nature Switzerland AG, ISBN: 978-3-030-43263-8, 2020.

[32] F. Salvat, A. Jablonski, C.J. Powell, Elsepa—Dirac partial-wave calculation of elastic scattering of electrons and positrons by atoms, positive ions and molecules, Comput. Phys. Comm. 165 (2) (2005) 157–190.

[33] C. Chaneliere, J. Autran, R. Devine, B. Balland, Tantalum pentoxide (Ta2O5) thin films for advanced dielectric applications, Mater. Sci. Eng. R (ISSN: 0927-796X) 22 (6) (1998) 269–322.

[34] J. Heyd, G.E. Scuseria, M. Ernzerhof, Hybrid functionals based on a screened Coulomb potential, J. Chem. Phys. 118 (18) (2003) 8207–8215.

[35] C. Adamo, V. Barone, Toward reliable density functional methods without adjustable parameters: The PBE0 model, J. Chem. Phys. 110 (13) (1999) 6158–6170.

[36] P. Giannozzi, et al., Advanced capabilities for materials modelling with quantum ESPRESSO, J. Physics. Condens. Matter 29 (46) (2017) 465901.

[37] E. Franke, C.L. Trimble, M.J. DeVries, J.A. Woollam, M. Schubert, F. Frost, Dielectric function of amorphous tantalum oxide from the far infrared to the deep ultraviolet spectral region measured by spectroscopic ellipsometry, J. Appl. Phys. 88 (9) (2000) 5166–5174.